PUBLISHED VERSION

Hill, Timothy James; Hamilton, Murray Wayne; Pieroux, D.; Mandel, P.
Intensity coherence of a multimode Nd-doped yttrium aluminum garnet laser Physical Review A, 2002; 66(6):063803-1-063803-8

© 2002 American Physical Society

http://link.aps.org/doi/10.1103/PhysRevA.66.063803

PERMISSIONS

http://publish.aps.org/authors/transfer-of-copyright-agreement

"The author(s), and in the case of a Work Made For Hire, as defined in the U.S. Copyright Act, 17 U.S.C.

§101, the employer named [below], shall have the following rights (the "Author Rights"):

[...]

3. The right to use all or part of the Article, including the APS-prepared version without revision or modification, on the author(s)' web home page or employer's website and to make copies of all or part of the Article, including the APS-prepared version without revision or modification, for the author(s)' and/or the employer's use for educational or research purposes."

15th March 2013

http://hdl.handle.net/2440/12725

Intensity coherence of a multimode Nd-doped yttrium aluminum garnet laser

T. Hill and M. W. Hamilton*
Department of Physics and Mathematical Physics, University of Adelaide, Adelaide SA 5005, Australia

D. Pieroux and P. Mandel†
Optique Nonlinéaire Théorique, Université Libre de Bruxelles, Campus Plaine, Code Postal 231, B-1050 Bruxelles, Belgium
(Received 3 October 2001; published 6 December 2002)

We measure the power spectral densities, at relaxation oscillation frequencies, of the individual longitudinal modes and the total intensity of a Nd-doped yttrium aluminum garnet laser at low pumping rate. We then test relationships between these quantities that are derived from the modal rate equations theory. The theoretical relations for the two mode case are confirmed by the experiment. However, in the three-mode regime, theory and experiments do not agree well.

DOI: 10.1103/PhysRevA.66.063803 PACS number(s): 42.65.Sf, 42.60.Mi, 42.60.Rn

I. INTRODUCTION

There has been much recent interest in the spectra of intensity fluctuations in multimode lasers because these lasers exemplify nonlinear oscillator arrays and because the spectra are a useful test of the theoretical models used for the lasers. One of the earliest and most well known models is that due to Tang, Statz, and deMars, referred to herein as TSD [1]. In this model a modal expansion of the inversion density (or the gain) is employed, with a rather arbitrary truncation being needed to arrive at the set of ordinary differential equations that constitutes the TSD model. Two other basic assumptions that go into the model are that the gain medium fills the cavity and that the gain is distributed uniformly along the axis of the laser. Other models which do not make these latter assumptions still, as a general rule, employ the same modal expansion as TSD [2–6]. A more general approach that eschews the modal expansion, using so-called global rate equations, was also developed [7]. These models do not incorporate the phase. At the level of the rate equations the phase variables obey an evolution equation that is decoupled from the equations that describe the intensity dynamics. To reconnect the phase and amplitude variable requires a deep revision of the adiabatic elimination of atomic polarization, which is performed in the rate equation derivation. This task is outside the scope of the present paper.

Whether in the single-mode or in the multimode regime, two frequency domains have to be distinguished. There are the optical frequencies, characterizing the cavity eigenmodes. They are shifted from the empty cavity frequencies as a result of the frequency pulling and pushing induced by the light-matter interactions. However, there are also the relaxation oscillation frequencies (ROF's) which are in the kHz to MHz range for common solid state lasers. In principle, there are as many ROF's as there are modes, although this is not an absolute rule [8]. When there is more than one ROF, the ROF originating from the single-mode regime is usually the one with the highest frequency, the others having typically about half that value. A feature of both the experimental data and the aforementioned models is the phenomenon of antiphasing. This occurs at the ROF's when there is destructive interference of the contributions of the individual laser cavity modes to the fluctuations of the total intensity. Simple quantitative expressions that relate the power spectral densities of modal intensity fluctuations to total intensity fluctuations have been derived for two- [9] and three- [10,11] mode operation of the laser. The relations describe how these interferences occur at each ROF, specifying which mode pairs interfere constructively and which interfere destructively. For example, in two-mode operation where there is only one-mode pair, at the lower ROF the modes are in antiphase (destructive interference) and at the higher frequency they constructively interfere. Thus if the destructive interference is complete there will only be one resonance seen in the power spectrum of total intensity fluctuations, that at the higher system frequency. It is important to stress that these interferences at the ROF's correspond physically to the fluctuations of the field intensity and not the complex field amplitude.

While these expressions are predicated on a particular laser model (i.e., TSD), they have a certain universality in the sense that they are independent of the detailed parameters of the laser, such as pump rate (insofar as operation with a given number of modes is maintained). A necessary condition for the derivation of these simple relations is that the lifetime of the cavity modes is much smaller than that of the population inversion. For solid state lasers with the Nd^{3+} ion as the active species this is generally the case. Experiments with a LNP (lithium neodymium tetraphosphate) laser [12], where these rates differ by a factor of about 10^6, have confirmed these relations. One purpose of this paper is to put forward another case where these relations are tested, but where the decay rates differ by a smaller factor. It will be seen that the relations are verified for two-mode operation but not for three mode. It is well known that the TSD model has limitations when applied to real lasers. In particular it assumes that the gain medium fills the cavity and that the pumping is uniform. Although neither of these apply to our laser, we persist with the TSD model because with this model the relations can be derived analytically. Relations

*Electronic address: mwh@physics.adelaide.edu.au
†Electronic address: pmandel@ulb.ac.be

 ©2002 The American Physical Society

have been analytically derived for the two-mode case with a rate equation model which takes into account the large scale nonuniformity of the pump [7], as one would find in an end-pumped laser, but do not so far appear to be possible for three modes or more, which is of particular interest here.

We use a multimode Nd:YAG (neodymium-doped yttrium aluminum garnet) laser, in which the upper state lifetime of the lasing transition is 230 μs [13] and the cavity lifetime is 2.0 ns. This latter value is derived from the ROF of the laser in single-mode operation. The ratio of decay rates is thus $\sim 1.1\times 10^5$. The laser is operated in steady state with either two or three longitudinal modes, in which the relaxation oscillations of the laser modes are globally coupled by gain sharing. For N laser modes there are N ROF's which occur up to the single-mode ROF [14], and are of the order of tens of kHz making their direct study relatively simple. The ROF's are excited only by ambient noise in this paper.

In Sec. II we review the theory behind antiphase dynamics of the multimode laser in the context of the TSD model, making explicit the connection between the experimentally obtained spectra and the variables of the theory. Then in Sec. III the experimental arrangement is described. Experimental results for the two-mode case are presented in Sec. IV and there it is demonstrated that they agree well with theoretical predictions of power spectral densities of the modal intensities at each of the ROF's. A confirmation of these results based on the cross-spectra between modal pairs is also presented. In contrast to Sec. IV, we present in Sec. V results from three-mode operation that show clear quantitative disagreement with the predictions of the theory based on the TSD model. The data suggest that in the correct model the relative phases of the modal intensity fluctuations will be different, but that power spectra relations similar to the ones introduced below will be obtained. Further, a recent comparison of a model incorporating nonuniform pumping with one that assumes uniform pumping shows that this aspect hardly affects the threshold properties of a laser [15]. This leads us to suspect that the assumption of pump uniformity is not the relevant limitation of the TSD model.

II. THEORETICAL RESULTS

A. The TSD model

In 1963, Tang, Statz, and deMars proposed a simple model to describe the dynamics of multilongitudinal mode Fabry-Perot class-B lasers [1]. Starting from a noiseless semiclassical laser description, the derivation of the model proceeds in three stages. Firstly, the medium polarization is adiabatically eliminated. This simplification holds if the polarization lifetime is much smaller that both the photon and population inversion lifetimes. This is in particular the case for the LNP, Nd:YAG, and semiconductor lasers. Then, the population inversion is spatially Fourier expanded. The last stage consists of discarding all but the first order Fourier components. For a N mode laser, this results in $2N+1$ nonlinear ordinary differential equations,

$$\begin{aligned}
\frac{dI_m}{dt} &= \kappa I_m[\,\gamma_m(N_0 - N_m/2) - 1\,],\\
\frac{dN_m}{dt} &= \gamma_m N_0 I_m - N_m\left(1 + \sum_{k=1}^{N} \gamma_k I_k\right),\\
\frac{dN_0}{dt} &= w - N_0 - \sum_{k=1}^{N} \gamma_k (N_0 - N_k/2) I_k\,,
\end{aligned} \tag{1}$$

with $m=1,\ldots,N$. In these equations, I_m is the intensity of mode m, N_0 and N_m are zero- and first-order spatial Fourier components of the population inversion, i.e.,

$$\begin{aligned}
N_0 &= \frac{1}{L}\int_0^L N(x,t)\,dx,\\
N_m &= \frac{2}{L}\int_0^L N(x,t)\cos(2k_m x)\,dx
\end{aligned} \tag{2}$$

with $N(x,t)$ the population inversion density, k_m the optical wave number of mode m, and L the cavity length. Time t is measured in units of the population inversion relaxation time, w is the pump parameter averaged over the cavity length, and $\gamma_m \leqslant 1$ is the gain of mode m relative to the maximum gain mode $m=1$. In what follows, we order the modes according to their lasing threshold value, or equivalently in the case of the TSD model such that $1=\gamma_1 > \cdots > \gamma_N$. Equality between two or more mode gains occurs in degenerate cases, but we do not consider this possibility here since it does not correspond to any of our experiments. The κ parameter is the inverse photon lifetime that we assume equal for all modes. One of the formal limitations of the TSD model is that it describes a homogeneously pumped medium filling the cavity over its whole length. More complex models have been recently proposed for a partially filled cavity or an inhomogeneous pump mechanism [6,7,16,17]. However, as the inhomogeneity of the inversion acts mainly on the strength of mode-mode competition, we expect the TSD model to give a qualitative description of the dynamics of inhomogeneously pumped lasers by using an effective pump value and effective mode gains.

As mentioned in the preceding section, κ for Nd:YAG lasers is about 10^5. For such a large value, and in the absence of parameter modulation, the TSD model displays fairly simple dynamics. For $w<1$, all modes are switched off. At $w=1$ the $m=1$ mode starts lasing, followed by the other modes as w increases further. Whatever the pump value, the system always possesses a single stable steady state such that modes whose threshold is below the current pump value are lasing while the other modes are not. If weakly perturbed, the laser returns to its stable steady state via damped oscillations. For an N mode laser with all unequal gains, N different relaxation frequencies $\omega_1 > \cdots > \omega_N$ are found in the power spectra of the relaxation transients of each mode.

For a small enough perturbation, Eqs. (1) can then be linearized. Solving the linear equations, the relaxation transient is given by

$$I_m(t) = I_{m,\mathrm{st}} + \sum_{k=1}^{N} (\epsilon_k a_{m,k} e^{(\gamma_k + i\omega_k)t} + \mathrm{c.c.}) + O(\epsilon^2), \quad (3)$$

with $I_{m,\mathrm{st}}$ being the steady intensity of mode m, $\gamma_k + i\omega_k$ the kth eigenvalue of the linear problem, and $a_{m,k}$ the amplitude of the mth component of the kth eigenvector. As all the γ_k are negative, the transient is damped. It is important to note that the coefficients $a_{m,k}$ are independent of the perturbation, contrary to the complex parameters ϵ_k that are univocally determined by it. Being linear, Eq. (3) applies also to the total intensity $I_{tot} = \Sigma_{m=1}^{N} I_m$ if the $a_{m,k}$ are replaced by $a_{\mathrm{tot},k} = \Sigma_{m=1}^{N} a_{m,k}$. The eigenvectors being defined up to a complex scaling factor, we choose $a_{\mathrm{tot},k}$ real and not negative for all k.

B. Fourier component relations

In the limit of large κ, the frequencies ω_k scale as $\kappa^{1/2}$ while the damping rates γ_k are of $\mathcal{O}(1)$ [18]. These two time scales lead to the existence of a range of durations T such that $\omega_k^{-1} \ll T \ll \gamma_k^{-1}$. That is, during a time T, the laser displays many oscillations without being significantly damped. This fact simplifies the computation of the ω_k components of the Fourier-transformed intensities over a limited duration T:

$$\mathcal{F}_T(I_m, \omega_k) = \int_0^T I_m(t) e^{-i\omega_k t} \mathrm{d}t \approx \epsilon_k a_{m,k} T. \quad (4)$$

This relation holds also for $\mathcal{F}_T(I_{tot}, \omega_k)$ if $a_{m,k}$ is replaced by $a_{\mathrm{tot},k}$. The set of relations (4) allows one to recover the eigenvectors of the linearized TSD system from the Fourier transform of the laser intensity time traces, since the ϵ_k and T parameters are easily eliminated to give

$$a_{m_1,k} \mathcal{F}_T(I_{m_2}, \omega_k) \approx a_{m_2,k} \mathcal{F}_T(I_{m_1}, \omega_k). \quad (5)$$

C. Power and cross-spectra relations

Checking the validity of the set of relations (5) is a difficult task as every $a_{m,k}$ depends on the pump w and the modal gain parameters γ_m. However, universal relations independent of the pump and the gains can be established using the power spectral densities (PSD) and cross-spectral densities (CSD) defined, respectively, by

$$\mathcal{P}_T(I_m, \omega_k) = \frac{1}{T} |\mathcal{F}_T(I_m, \omega_k)|^2, \quad (6)$$

$$\mathcal{C}_T(I_m, I_n, \omega_k) = \frac{1}{T} \mathcal{F}_T(I_m, \omega_k) \mathcal{F}_T^*(I_n, \omega_k), \quad (7)$$

with the asterisk denoting the complex conjugate. To derive these relations, it is necessary to refer to two properties of the $a_{m,k}$ coefficients that hold in the limit $\kappa \gg 1$. The first property is that all $a_{m,k}$ can be chosen real in a first approximation. This comes from the fact that $\mathrm{Re}(a_{m,k}) \sim \kappa^{1/2} \mathrm{Im}(a_{m,k})$. This fundamental property is at the origin of the antiphase laser dynamics, i.e., the absence or the strong reduction of the $\omega_2, \ldots, \omega_N$ frequency peaks in the total intensity transient. Indeed, the set of N modes is divided in two clusters for each ω_k: the N' modes whose $a_{m,k}$ are positive, and the $N - N'$ modes whose $a_{m,k}$ are negative. Modes belonging to the first cluster oscillate in phase, but they oscillate out of phase (i.e., phase shifted by π) with the modes of the other cluster. Therefore, the total intensity oscillates with an amplitude resulting from the contribution of the first cluster reduced by the contribution of the second one. The second property of $a_{m,k}$ is that above the threshold of mode m, all $\mathrm{sgn}(a_{m,k})$ are constant. These are given in Table I for three-mode operation. These two properties have been demonstrated for any N and $\gamma_m \approx 1$ [19], for $N = 2$ and any γ_m [12], and for $N = 3$ and any γ_m [11], but we conjecture that they are valid for any N and any γ_m. It is now straightforward to show that

$$\sqrt{\mathcal{P}_T(I_{tot}, \omega_k)} = \sum_m \mathrm{sgn}(a_{m,k}) \sqrt{\mathcal{P}_T(I_m, \omega_k)}, \quad (8)$$

and

$$\arg[\mathcal{C}_T(I_m, I_n, \omega_k)] = \begin{cases} 0 & \text{if } \mathrm{sgn}(a_{m,k}) = \mathrm{sgn}(a_{n,k}) \\ \pi & \text{otherwise.} \end{cases} \quad (9)$$

These relations are universal since they hold whatever the perturbation, the pump or the gain parameters. Table II illustrates Eq. (9) for all m, n, and k, in the case $N = 3$. Equations (8) and (9) describe interference of the modal intensity fluctuations. If $\arg[\mathcal{C}_T(I_m, I_n, \omega_k)] = \pi$, modes m and n are in antiphase; that is, their fluctuations at ω_k interfere destructively.

TABLE I. Sign of the $a_{m,k}$ coefficients as predicted by the TSD model for three-mode operation. The two-mode case is obtained by removing the $a_{3,k}$ row and the ω_3 column.

	ω_1	ω_2	ω_3
$a_{1,k}$	+	−	−
$a_{2,k}$	+	+	−
$a_{3,k}$	+	+	+
$a_{\mathrm{tot},k}$	+	+	+

TABLE II. Theoretical prediction of the cross-spectra complex phase $\arg[\mathcal{C}(I_m, I_n, \omega_k)]$ for three-mode operation. The two-mode case is obtained by removing the row and the column labeled I_3, as well as the three columns corresponding to ω_3. A null value indicates that modes m and n oscillate in phase, while π means that they oscillate with opposite phase. These results follow immediately from Eq. (9) and Table I.

	ω_1			ω_2			ω_3		
	I_1	I_2	I_3	I_1	I_2	I_3	I_1	I_2	I_3
I_1	0	0	0	0	π	π	0	0	π
I_2	0	0	0	π	0	0	0	0	π
I_3	0	0	0	π	0	0	π	π	0
I_{tot}	0	0	0	π	0	0	π	π	0

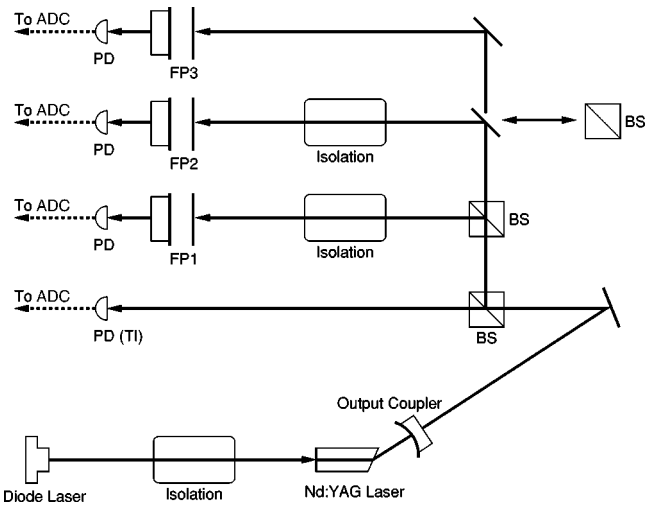

FIG. 1. Schematic of the optical part of the experimental setup for two-mode operation. ADC, analog to digital converter; PD, photodiode; TI, total intensity; FP1, Fabry-Perot 1; FP2, Fabry-Perot 2; FP3, Fabry-Perot 3; BS, beam splitter. For three-mode operation, one mirror is replaced by a BS as indicated.

D. Application to noisy lasers

In practice, every laser is a noisy device. The noise originates from the spontaneous emission (quantum noise) and from environmental perturbations. Modeling the noise properties of an experimental Nd:YAG laser system is a formidable task, out of the scope of this paper. Therefore, we choose to use a qualitative approach by modeling the noise effect as a series of instantaneous, independent and random kicks that perturb the laser. Right after a kick, the laser relaxes towards its steady state, until it is pushed again by yet another kick. If the noise level is weak, the laser remains in the neighborhood of its stable steady state and the linear theory we have developed previously applies. The dynamics of the laser between two kicks is then described by Eq. (3), with each ϵ_k being a random constant that is updated after each kick. If the average duration T between two kicks is such that $\omega_k^{-1} \ll T \ll \gamma_k^{-1}$, the relations (8) and (9) still hold since they are independent of the perturbation. Moreover, the laser does not have enough time to relax to its steady state before being perturbed again. Therefore, the upper integration bound of Eq. (4) can be taken much larger than T. As a result, long time traces are appropriate to compute the PSD's and the CSD's.

III. EXPERIMENTAL SETUP

Our Nd:YAG laser (Nd$\sim$1% concentration) is end pumped by a 40 mW diode laser operating at 808 nm; see Fig. 1. The YAG rod is 10 mm long and 3 mm in diameter. It is perpendicularly cut at the front face and Brewster cut at the other to force linear polarization, ensuring that the laser system does not exhibit polarization instability and switching [20]. The front face of the YAG rod forms one end of the cavity; it is highly reflective at 1064 nm and partially reflecting (R$\sim$30%) at 808 nm. Optical isolation (measured to be approximately 35 dB) with a polarizing beam splitter and a Fresnel rhomb was used between the YAG rod and the laser diode to minimize instabilities in the diode. At the other end of the YAG laser cavity is a spherical output coupling mirror (R$\sim$98% at 1064 nm) with radius of curvature 2.5 cm. The output coupling mirror was chosen for relatively low frequency relaxation oscillations rather than high output power. The output power is of order 1 mW. The optical length of the cavity is approximately 2.5 cm giving rise to a measured longitudinal mode spacing of 6.15 GHz. The laser operates on the 1064 nm transition with up to six longitudinal modes, depending on the exact cavity length and pump power. The output beam had a good TEM_{00} transverse intensity profile. The output coupler was mounted on a piezoelectric transducer to allow fine control of the cavity length, so that we could offset the laser mode spectrum with respect to the gain spectrum and actively control its length with a servo-loop.

Figure 1 shows the optical setup for two-mode operation. The laser cavity modes were separated using Fabry-Perot interferometers. Optical isolation with quarter wave plates and polarizing beam splitters (measured to be approximately 28 dB) was used between the YAG laser and the Fabry-Perots. The modal and total intensities were detected with identical high gain, low noise photodiode-amplifier circuits (Photodiodes - Epitaxx, ETX 1000T). With up to four detection channels, each modal intensity and the total intensity could be sampled simultaneously. Simultaneous sampling minimizes the effect of the thermal drift of the Nd:YAG laser cavity by keeping the time scale of the measurement short (525 ms), and allows a determination of the scaling of each optical channel. We can then compare the measured total intensity (TI) directly with the summed modal intensities, which is a useful test of our method.

The intensities were recorded with two, 12 bit, 2 channel analog to digital converters (ADC's) (Gage Applied Sciences Inc., CompuScope 512) mounted in separate PC's. Each of the input channels recorded 2^{19} points at a sample rate of 1 MS/s. The sampling interval was much shorter than the period of highest ROF ($\sim$20 μs) and the number of recorded points gave an adequate amount of data for averaging in the frequency domain. Once the appropriate input range of the ADC was selected, extra gain was applied directly after the photodiode-amplifiers to maximize the signal-to-noise ratio (SNR) and resolution of the data. The recorded intensity data was transformed into the frequency domain (i.e., power or cross-spectrum) using the modified periodigram method [21].

An aluminum spacer was used in the Nd:YAG laser cavity. Due to thermal expansion, the frequencies of the laser modes and their associated gains could change. We temperature stabilized the laser cavity to minimize this effect. One Fabry-Perot (FP1) (TecOptics Ltd., SA-10 with a cavity lifetime of approximately 4.25 ns) was spaced with Invar which has a much lower coefficient of expansion than aluminum. In the experiments we used it as a reference cavity to which we actively stabilized one of the laser cavity modes (the first to reach threshold) and therefore the laser cavity length. This fixed the position of the cavity modes with respect to the peak of the gain spectrum, and thus the relative gains of the modes. We did this by applying a very low level dither to the

piezoelectric transducer of FP1 at 1251 Hz which is far enough away in frequency from the ROF's of the laser to be easily distinguishable when it appears in the power and cross-spectra. A lock-in amplifier generated an error signal from the intensity of the first laser mode to reach threshold which in turn was fed back to the output coupler of the YAG laser cavity. The combination of active stabilization of the laser cavity and simultaneous sampling of all intensities maintained a constant position of the laser cavity modes with respect to the gain spectrum for the duration of the experiment. The other Fabry-Perot (FP2) (cavity lifetime of approximately 230 ps) was also dithered and, with a secondary feedback loop, locked to the laser cavity mode it transmitted (i.e., the second to reach threshold).

For three-mode operation, the system was extended with the addition of a third Fabry-Perot (FP3) (cavity lifetime of approximately 480 ps), see Fig. 1. This Fabry-Perot transmitted the third laser cavity mode to reach threshold. In two-mode operation FP2 was locked to the laser mode that it transmitted, using the same technique that was used for stabilizing the laser cavity to FP1. In fact the data was acquired in about 0.5 s and the drift of FP2, without stabilization, in this time proved to be negligible. Thus for three-mode operation we did not lock FP2 or FP3 to the modes that they transmitted. The photodiode-amplifier circuit used to detect the intensity from FP3 was identical to those used previously. After further gain, this signal was fed into the fourth available channel of the ADC's.

For both two- and three-mode operation, the relative gains of the laser cavity modes were always chosen to be unequal. To do this we offset the laser mode spectrum with respect to the gain spectrum while viewing the laser modes with a Fabry-Perot used as an optical spectrum analyzer.

In both operation regimes, each optical channel had a different amount of light impinging on the photodetector. To make accurate calculations (and for comparing our data with other results [9–12]), it is therefore important to determine the appropriate scaling for each optical channel. This was done by starting the laser in single-mode operation (each time an experiment was performed) and recording that mode with each channel. The standard deviation of the intensity noise was calculated from the data and the scalings found. Therefore in both two- and three-mode operation, the intensity series were normalized to one of the optical channels before transformation into the frequency domain.

For each operating point the total intensity and the modal intensities were recorded. The power spectral densities of the fluctuations of each of the total intensity, the sum of modal intensities, and the individual modal intensities were calculated. The sum of modal intensities, and its power spectrum, were calculated as a check of the scaling of the different recording channels. Cross-spectra were also calculated for pairs of modal intensities.

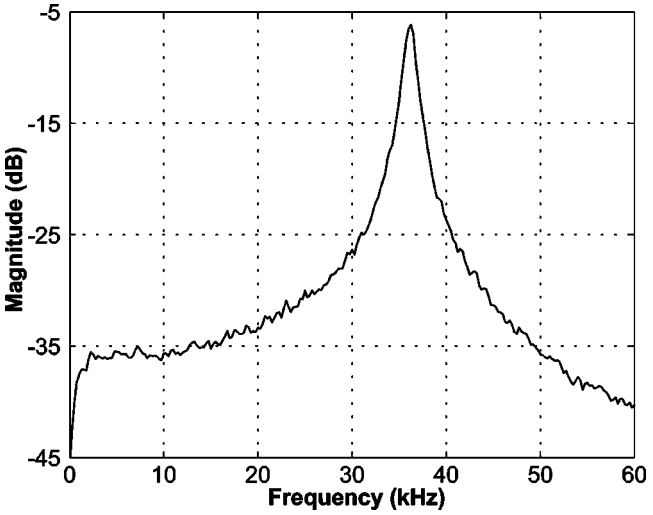

FIG. 2. Power spectrum of the total intensity noise fluctuations, two-mode operation. The system ROF's are 7.50 and 36.25 kHz.

IV. TWO-MODE OPERATION

In this section we use data recorded by our experimental setup working in two-mode operation to check the validity of the relations (8) and (9). The data set has been obtained for a pump value $w=1.022$, the first mode threshold being $w_1=1$ by definition and the second mode threshold being located at $w_2=1.010$. The two relaxation frequencies, $\omega_1 \approx 36.25$ kHz and $\omega_2 \approx 7.50$ kHz, have been determined from the location of the resonant peaks of a modal intensity power spectrum. The PSD of the directly measured total intensity is shown in Fig. 2. The observed peak is located at ω_1 and has a full width at half maximum of 1.22 kHz. No peak is apparent at ω_2, the PSD being made of a superposition of noise and the low frequency wing of the ω_1 peak. The ω_1 and ω_2 PSD values computed from the experimental time traces of I_1, I_2, and I_{tot} are given in Table III. To check the consistency and the precision of our measurement, we also computed the PSD of I_1+I_2. The last column of Table III is obtained by application of the relations (8) that, in the two-mode case, reduce to [12]

$$\sqrt{\mathcal{P}_{\mathrm{TSD}}(I_{tot},\omega_1)}=\sqrt{\mathcal{P}(I_2,\omega_1)}+\sqrt{\mathcal{P}(I_1,\omega_1)},$$

$$\sqrt{\mathcal{P}_{\mathrm{TSD}}(I_{tot},\omega_2)}=\sqrt{\mathcal{P}(I_2,\omega_2)}-\sqrt{\mathcal{P}(I_1,\omega_2)}. \qquad (10)$$

TABLE III. Power spectral densities for two-mode operation: $\mathcal{P}(I_1)$, $\mathcal{P}(I_2)$, $\mathcal{P}(I_{tot})$ correspond, respectively, to the measured modal and total intensity fluctuations, $\mathcal{P}(I_1+I_2)$ is computed by summing the fluctuation time traces of the two modal intensities, and $\mathcal{P}_{\mathrm{TSD}}(I_{tot})$ is obtained by application of Eq. (8).

	$\mathcal{P}(I_1)$	$\mathcal{P}(I_2)$	$\mathcal{P}(I_{tot})$	$\mathcal{P}(I_1+I_2)$	$\mathcal{P}_{\mathrm{TSD}}(I_{tot})$
ω_1	0.14774	0.01301	0.24136	0.24837	0.24844
ω_2	0.00538	0.00619	0.00029	0.00033	2.85×10^{-5}

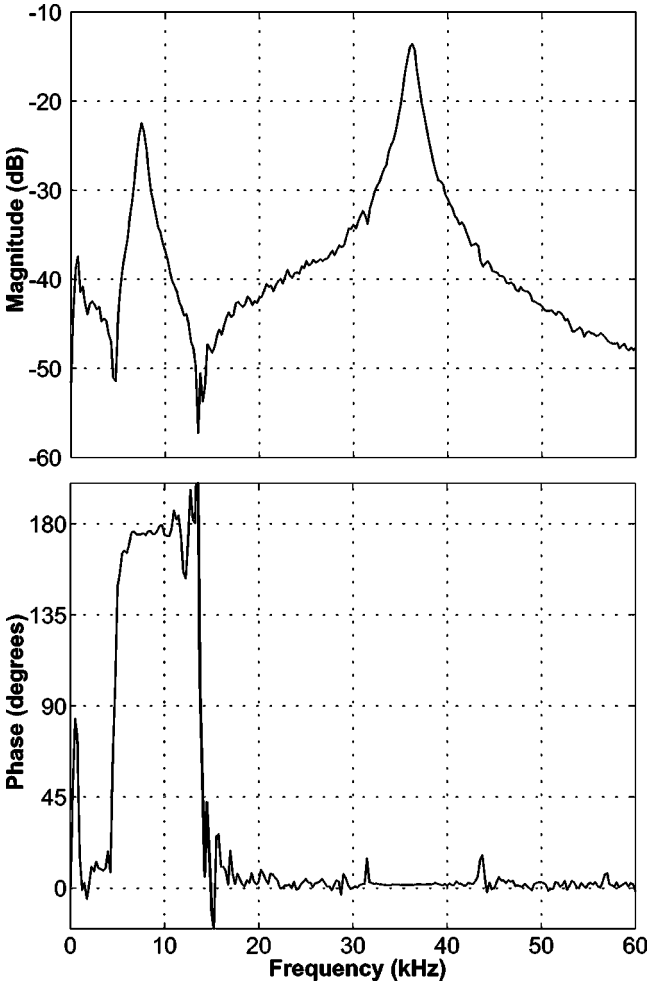

FIG. 3. Cross-spectrum of intensity noise fluctuations between laser modes 1 and 2, for two-mode operation. The ROF's are 7.50 and 36.25 kHz. Phase jumps occur at approximately 4.75 and 13.5 kHz. A weak dither signal (1251 Hz) can be seen in the magnitude. Electronic pickup from switch mode power supplies can be seen in the phase at approximately 32 and 44 kHz.

In Table III it is seen that $\mathcal{P}(I_{tot},\omega_1)$, $\mathcal{P}(I_1+I_2,\omega_1)$, and $\mathcal{P}_{\mathrm{TSD}}(I_{tot},\omega_1)$ are in a very good agreement, their relative differences being smaller than 3%. At first sight, the situation is far from being that good at ω_2: while $\mathcal{P}(I_{tot},\omega_2)$ and $\mathcal{P}(I_1+I_2,\omega_2)$ differ by a mere 13%, $\mathcal{P}_{\mathrm{TSD}}(I_{tot})$ is ten times smaller. However, this is only an apparent problem that can be rather well explained. Indeed, $\mathcal{P}_{\mathrm{TSD}}(I_{tot},\omega_2)\approx 3\times 10^{-5}$ suggests that a very strong antiphase dynamics cancels most of the ω_2 oscillation in the total intensity. Therefore, $\mathcal{P}(I_{tot},\omega_2)$ and $\mathcal{P}(I_1+I_2,\omega_2)$ mainly measure the background noise intensity, leading to $\mathcal{P}_{\mathrm{TSD}}(I_{tot},\omega_2) < \mathcal{P}(I_{tot},\omega_2)\approx\mathcal{P}(I_1+I_2,\omega_2)\ll 1$ which is exactly the situation illustrated in Table III.

Using the cross-spectral method [22], the phase pattern between the two modes has been calculated, see Fig. 3. At ω_1, the cross-spectral phase is approximately zero, meaning that the two modes are oscillating in phase. With decreasing ω, the phase of the cross-spectrum changes abruptly from 0 to π at about $\omega=15$ kHz, leading to antiphase dynamics at ω_2. This result is consistent with the relations (10) and confirms the content of Table II limited to 2 modes.

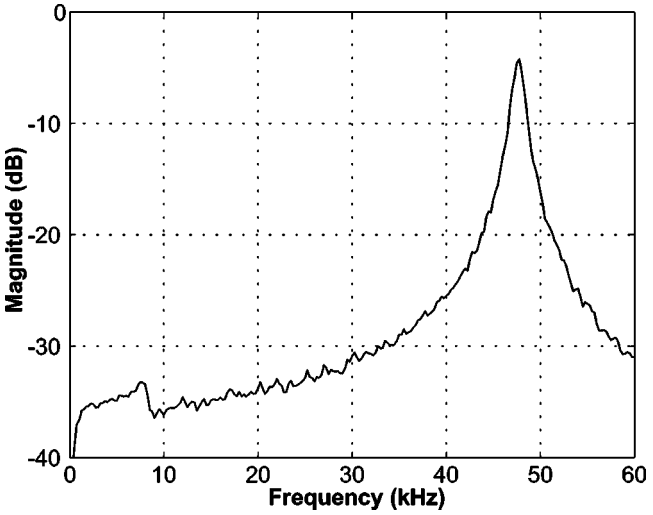

FIG. 4. Power spectrum of the total intensity noise fluctuations for three-mode operation. The ROF's are 8.00, 11.75, and 47.75 kHz.

This experiment and analysis have been repeated with success for different pump levels and mode gains. We therefore conclude that the relations (8) and (9) hold for Nd:YAG lasers in two-mode operation.

V. THREE-MODE OPERATION

We consider now data obtained by operating our Nd:YAG laser system with three modes. The third mode threshold is located at $w=1.024$ and we operate the laser at $w=1.037$. The laser relaxation frequencies are $\omega_1\approx 47.75$ kHz, $\omega_2\approx 11.75$ kHz, and $\omega_3\approx 8.00$ kHz. The total intensity power spectrum is shown in Fig. 4. The ω_1 peak is clearly visible, while a vestige of the ω_3 peak is observed 1 to 2 dB above the background noise. It is very weak in comparison with the ω_1 peak. No peak is distinguishable at ω_2. The theoretical values of $\mathrm{sgn}(a_{m,k})$ are given in Table I, so that Eqs. (8) reduce to [11]

$$\sqrt{\mathcal{P}_{\mathrm{TSD}}(I_{tot},\omega_1)}=\sqrt{\mathcal{P}(I_3,\omega_1)}+\sqrt{\mathcal{P}(I_2,\omega_1)}+\sqrt{\mathcal{P}(I_1,\omega_1)}, \tag{11a}$$

$$\sqrt{\mathcal{P}_{\mathrm{TSD}}(I_{tot},\omega_2)}=\sqrt{\mathcal{P}(I_3,\omega_2)}+\sqrt{\mathcal{P}(I_2,\omega_2)}-\sqrt{\mathcal{P}(I_1,\omega_2)}, \tag{11b}$$

$$\sqrt{\mathcal{P}_{\mathrm{TSD}}(I_{tot},\omega_3)}=\sqrt{\mathcal{P}(I_3,\omega_3)}-\sqrt{\mathcal{P}(I_2,\omega_3)}-\sqrt{\mathcal{P}(I_1,\omega_3)}. \tag{11c}$$

The experimental PSD's computed from the laser intensity time traces and the theoretical predictions of the TSD model are reported in Table IV. The agreement between the PSD's obtained by using the measured total intensity and by summing the modal intensity time traces (columns four and five) is not as good as in the two-mode case, despite careful efforts in measuring the sensitivity of each optical channel. The relative differences between these two estimates of the

TABLE IV. Power spectral densities for three-mode operation: $\mathcal{P}(I_1)$, $\mathcal{P}(I_2)$, $\mathcal{P}(I_3)$, $\mathcal{P}(I_{tot})$ correspond, respectively, to the measured modal and total intensity fluctuations. $\mathcal{P}(I_1+I_2+I_3)$ is computed by summing the fluctuation time traces of the three modal intensities. $\mathcal{P}_{\mathrm{TSD}}(I_{tot})$ is computed from Eq. (8) and $\mathcal{P}^{\mathrm{corr.}}_{\mathrm{TSD}}(I_{tot})$ from Eq. (12).

	$\mathcal{P}(I_1)$	$\mathcal{P}(I_2)$	$\mathcal{P}(I_3)$	$\mathcal{P}(I_{tot})$	$\mathcal{P}(I_1+I_2+I_3)$	$\mathcal{P}_{\mathrm{TSD}}(I_{tot})$	$\mathcal{P}^{\mathrm{corr.}}_{\mathrm{TSD}}(I_{tot})$
ω_1	0.11626	0.02957	0.00886	0.37732	0.32585	0.36850	0.36851
ω_2	0.00225	0.00879	0.00217	0.00031	0.00077	0.00863	6.536×10^{-8}
ω_3	0.01687	0.00327	0.00628	0.00045	0.00071	0.01163	4.33×10^{-5}

total intensity PSD's are 16%, 150%, and 56% at ω_1, ω_2, and ω_3, respectively. The large discrepancies at ω_2 and ω_3 can be partially explained by the small ratio of the signal to background noise. Nevertheless, there is an agreement on the magnitude of the PSD's. The theoretical estimation $\mathcal{P}_{\mathrm{TSD}}(I_{tot},\omega_1)$ matches well with $\mathcal{P}(I_{tot},\omega_1)$ (a 2% error) and $\mathcal{P}(I_1+I_2+I_3,\omega_1)$ (a 13% error). However, $\mathcal{P}_{\mathrm{TSD}}(I_{tot},\omega_2)$ and $\mathcal{P}_{\mathrm{TSD}}(I_{tot},\omega_3)$ are much larger than their corresponding experimental values. Thus the TSD model fails to verify the PSD relations for our three-mode laser setup.

Nevertheless, by analyzing the experimental cross-spectral figures, it appears that the intensity components of the eigenvectors can still be chosen real, as predicted by the TSD model in the asymptotic limit of κ large. We report the experimental evaluation of all $\mathrm{sgn}(a_{m,k})$ in Table V. Before analyzing this table in depth, we have to explain the self-inconsistency found amongst its ω_2-column entries. According to the table, I_1 and I_2 are oscillating out of phase (i.e., phase shifted by π in this case), while simultaneously oscillating in phase with the total intensity. This is most probably caused by the small amplitude of the total intensity at ω_2 relative to the background noise. Therefore, we decide not to take into consideration the ω_2 entries of the total intensity row. To remain consistent, we also do not consider the ω_3 entries of the total intensity row since they could also be similarly affected. Even with these entries removed, the remaining underlined entries of Table V are opposite to the theoretical predictions of Table II. Obviously, these differences result from the inadequacy of the TSD model to describe the structure of our Nd:YAG laser system. Contrary to the hypotheses of the TSD model, (1) our laser active medium does not fill in the whole cavity, and (2) it is end-pumped and the pumping power decreases exponentially along the medium. These features affect the laser dynamics but they are not taken into account in the TSD model. This leads to clear discrepancies between the TSD model predictions and the experimental observations. For instance, we have observed in some experiments that the second mode becomes brighter than the first one once the pump is strong enough. Increasing the pump further can make the third mode to reach threshold the most intense. These observations cannot be explained in the frame of the TSD model and show that we are out of its range of validity.

TABLE V. Experimental measures of the cross-spectra complex phase $\arg[\mathcal{C}(I_m,I_n,\omega_k)]$ for three modes. A null value indicates that modes *m* and *n* oscillate in phase, while π means that they oscillate with opposite phase. Terms in opposition with Table II are underlined.

	ω_1			ω_2			ω_3		
	I_1	I_2	I_3	I_1	I_2	I_3	I_1	I_2	I_3
I_1	0	0	0	0	π	0	0	π	π
I_2	0	0	0	π	0	$\underline{\pi}$	π	$\underline{0}$	0
I_3	0	0	0	0	π	$\underline{0}$	$\underline{\pi}$	0	$\underline{0}$
I_{tot}	0	0	0	$\underline{0}$	$\underline{0}$	$\underline{\pi}$	π	$\underline{0}$	0

Knowing that the entries of Table II are not all verified by the experiment, we rewrite Eqs. (8) using the experimental values of Table V. They become

$$\sqrt{\mathcal{P}^{\mathrm{corr.}}_{\mathrm{TSD}}(I_{tot},\omega_1)}=\sqrt{\mathcal{P}(I_3,\omega_1)}+\sqrt{\mathcal{P}(I_2,\omega_1)}+\sqrt{\mathcal{P}(I_1,\omega_1)},$$

$$\sqrt{\mathcal{P}^{\mathrm{corr.}}_{\mathrm{TSD}}(I_{tot},\omega_2)}=\sqrt{\mathcal{P}(I_3,\omega_2)}-\sqrt{\mathcal{P}(I_2,\omega_2)}+\sqrt{\mathcal{P}(I_1,\omega_2)},$$

$$\sqrt{\mathcal{P}^{\mathrm{corr.}}_{\mathrm{TSD}}(I_{tot},\omega_3)}=-\sqrt{\mathcal{P}(I_3,\omega_3)}-\sqrt{\mathcal{P}(I_2,\omega_3)}+\sqrt{\mathcal{P}(I_1,\omega_3)}. \tag{12}$$

These redefined total PSD's are shown in Table IV in column seven. Note that $\mathcal{P}^{\mathrm{corr.}}_{\mathrm{TSD}}(I_{tot},\omega_1)$ is unchanged relative to Eq. (11a). As already mentioned above, $\mathcal{P}^{\mathrm{corr.}}_{\mathrm{TSD}}(I_{tot},\omega_1)$ matches well with the experimental value. On the other hand, Table IV shows that $\mathcal{P}^{\mathrm{corr.}}_{\mathrm{TSD}}(I_{tot},\omega_2)$ and $\mathcal{P}^{\mathrm{corr.}}_{\mathrm{TSD}}(I_{tot},\omega_3)$ are now smaller than the corresponding experimental values; however, this can be explained with the arguments put forward in the two-mode case. Note that $\sqrt{\mathcal{P}^{\mathrm{corr.}}_{\mathrm{TSD}}(I_{tot},\omega_3)}$ is small but negative. This is due to the experimental noise that affects the measured functions and is of no significance here.

VI. CONCLUDING REMARKS

The good agreement in the two-mode case between the experimental data and the theory based on TSD is not too surprising because of the very restricted range of possibilities for the relative phase of the modal fluctuations. Thus the two-mode case is a check of the experimental technique

rather than being a check of a theoretical model. It is in the case of three (or more) modes, with the wider range of possibilities for relative phase, that the cross-spectral measurements serve as a sensitive test of theoretical models as shown in Sec. V. The result is that the TSD rate equations fail to give the correct answer because some essential information is not used.

ACKNOWLEDGMENTS

This work has been financially supported by the Australian Research Council, The University of Adelaide, the Fonds National de la Recherche Scientifique and the Interuniversity Attraction Pole Program of the Belgian government.

[1] C.L. Tang, H. Statz, and G. deMars, J. Appl. Phys. **34**, 2289 (1963).
[2] E.S. Kovalenko and L.I. Shangina, Izvestiya VUZ. Radiofizika **12**, 846 (1969) [Radiophys. Quantum Electron. **12**, 674 (1969)].
[3] O.N. Evdokimova and L.N. Kaptsov, Kvant. Elektron. **16**, 1557 (1989) [Sov. J. Quantum Electron. **19**, 1001 (1989)].
[4] G. Kozyreff and P. Mandel, Phys. Rev. A **58**, 4946 (1998).
[5] K. Otsuka, E.A. Viktorov, and P. Mandel, Europhys. Lett. **45**, 307 (1999).
[6] N.B. Abraham, L. Sekaric, L.L. Carson, V. Seccareccia, P.A. Khandokhin, Ya.I. Khanin, I.V. Koryukin, and V. G Zhislina, Phys. Rev. A **62**, 013810 (2000).
[7] P. Mandel, Eur. Phys. J. D **8**, 431 (2000).
[8] P.A. Khandokhin, P. Mandel, I.V. Koryukin, B.A. Nguyen, and Ya.I. Khanin, Phys. Lett. A **235**, 248 (1997).
[9] P. Mandel and J.Y. Wang, Phys. Rev. Lett. **75**, 1923 (1995); **76**, 1403(E) (1996).
[10] B.A. Nguyen and P. Mandel, Phys. Rev. A **54**, 1638 (1996).
[11] P. Mandel, B.A. Nguyen, and K. Otsuka, Quantum Semiclassic. Opt. **9**, 365 (1997).
[12] P. Mandel, K. Otsuka, J.Y. Wang, and D. Pieroux, Phys. Rev. Lett. **76**, 2694 (1996).
[13] W. Koechner, *Solid-State Laser Engineering*, 4th ed.(Springer, Berlin, 1996).
[14] D.E. McCumber, Phys. Rev. **141**, 306 (1966).
[15] I.V. Koryukin and P. Mandel, **4**, 27 (2002).
[16] D. Pieroux and P. Mandel, Quantum Semiclassic. Opt. **9**, L17 (1997).
[17] P.A. Khandokhin, E.A. Ovchinnikov, and E.Yu. Shirokov, Phys. Rev. A **61**, 053807 (2000).
[18] P. Mandel, M. Georgiou, K. Otsuka, and D. Pieroux, Opt. Commun. **100**, 341 (1993).
[19] D. Pieroux and P. Mandel, Opt. Commun. **107**, 245 (1994).
[20] C. Serrat and N.B. Abraham, Quantum Semiclassic. Opt. **10**, 197 (1998).
[21] W. H. Press, B. P. Flannery, S. Teukolsky, and W. Vetterling, *Numerical Recipes:The Art of Scientific Computing* (Cambridge University Press, New York, 1986).
[22] T. Hill, L. Stamatescu, and M.W. Hamilton, Phys. Rev. E **61**, R4718 (2000).